Proceedings of ASME Turbo Expo 2011
GT2011
June 6-10, 2011, Vancouver, British Columbia, Canada

GT2011-45105

DETERMINATION OF THE HEAT RELEASE DISTRIBUTION IN TURBULENT FLAMES BY A MODEL BASED CORRECTION OF OH* CHEMILUMINESCENCE

Martin Lauer*
Mathieu Zellhuber
Thomas Sattelmayer
Lehrstuhl für Thermodynamik
Technische Universität München
D-85747 Garching, Germany
Email: lauer@td.mw.tum.de

Christopher J. Aul
Department of Mechanical Engineering
Texas A&M University
College Station, Texas, 77843

ABSTRACT

Imaging of OH or CH* chemiluminescence with intensified cameras is often employed for the determination of heat release in premixed flames. Proportionality is commonly assumed, but in the turbulent case this assumption is not justified. Substantial deviations from proportionality are observed, which are due to turbulence-chemistry interactions. In this study a model based correction method is presented to obtain a better approximation of the spatially resolved heat release rate of lean turbulent flames from OH* measurements. The correction method uses a statistical strain rate model to account for the turbulence influence. The strain rate model is evaluated with time-resolved velocity measurements of the turbulent flow. Additionally, one-dimensional simulations of strained counterflow flames are performed to consider the non-linear effect of turbulence on chemiluminescence intensities. A detailed reaction mechanism, which includes all relevant chemiluminescence reactions and deactivation processes, is used. The result of the simulations is a lookup table of the ratio between heat release rate and OH* intensity with strain rate as parameter. This lookup table is linked with the statistical strain rate model to obtain a correction factor which accounts for the non-linear relationships between OH* intensity, heat release rate, and strain rate. The factor is then used to correct measured OH* intensities to obtain the local heat release rate. The corrected intensities are compared to heat release distributions which are measured with an alternative method. For all investigated flames in the lean, partially premixed regime the corrected OH* intensities are in very good agreement with the heat release rate distributions of the flames.*

NOMENCLATURE

C	Proportionality factor
D	Burner nozzle diameter [mm]
N	Number of measurements [-]
R	Two-point correlation function
T	Temperature [K]
X	Mole fraction [-]
a	Tangential strain rate of a material surface $[\frac{1}{s}]$
c	Time averaged reaction progress of combustion [-]
c_p	Isobaric heat capacity $[\frac{kJ}{kg \cdot K}]$
d	Burner center body diameter [mm]
$\vec{e}_i$	Unit vector [-]
i	Volumetric intensity
l_t	Turbulent length scale [m]
l_λ	Taylor length scale [m]
p	probability density function [-]
$\dot{q}$	Volumetric heat release rate $[\frac{W}{m^3}]$
r	Radial coordinate [mm]
r_i	Distance [mm]
u	Flow velocity $[\frac{m}{s}]$
u_l	Laminar flame speed $[\frac{m}{s}]$
v_η	Kolmogorov velocity $[\frac{m}{s}]$

*Address all correspondence to this author.

x	Axial coordinate [mm]
α	Tangential strain rate of a randomly oriented surface [$\frac{1}{s}$]
ε	Dissipation rate of turbulent kinetic energy [$\frac{m^2}{s^3}$]
λ	Wavelength [nm]
ν	Kinematic viscosity [$\frac{m^2}{s}$]
ρ	Density [$\frac{kg}{m^3}$]
σ	Standard deviation
τ_η	Kolmogorov time scale [s]
ϕ	Equivalence ratio [-]
$'$	Turbulent fluctuation
$\langle\rangle$	Averaged quantity
$\langle\rangle_t$	Time averaged quantity
$\langle\rangle_a$	Strain averaged quantity

INTRODUCTION

An important property of combustion systems is the heat release rate distribution of the flame. For lean premixed combustion, the knowledge of the local heat release rate is particularly important to understand, predict, and control unstable combustion states, such as thermoacoustic instabilities [1–3] and flame flashback [4, 5]. Also in partially premixed and non-premixed combustion systems, the heat release rate distribution is an important parameter in current research, for example for phenomena like combustion noise [6, 7], combustor design, and pollutant emission. However, the experimental determination of turbulent flame heat release rate is problematic, because available temporally and spatially resolved measurement techniques, like heat release imaging [8], are too complex to be applied to research fields like thermoacoustics [9].

Motivation

A common, easy-to-use indirect measure for the heat release distribution of a flame is its light emission, the so-called chemiluminescence. It has been shown in several studies that the integral emissions of chemiluminescent species like OH* or CH* are reliable measures for the integral heat release rate of flames [10–14]. Furthermore, it was shown that in laminar flames the spatially resolved OH* chemiluminescence is a measure for the spatially resolved heat release rate [8, 15].

However, a recent study by Lauer and Sattelmayer [16] demonstrated that the spatially resolved heat release rate of a turbulent flame cannot be obtained from chemiluminescence. The study used measurements from particle image velocimetry (PIV), planar laser induced fluorescence of the hydroxyl radical (OH-PLIF), and chemiluminescence as input parameters to evaluate an energy balance, which was derived from the first law of thermodynamics. The time averaged, spatially resolved heat release rate in the flame mid-plane was obtained and compared with the spatially resolved chemiluminescence intensities. It was shown that although the integral chemiluminescence intensity of the flame can be correlated with the integral heat release rate, neither OH* nor CH* are reliable measures for the spatially resolved heat release rate in turbulent flames.

The observed differences between chemiluminescence and heat release was due to large variations of the local turbulence intensity within the reaction zone of the flame. The chemiluminescence intensities are suppressed in regions with high turbulence, similar to the effects reported by John and Summerfield [11]. In turbulent swirl flames the highest turbulence intensities occur close to the burner exit. Therefore, the described effect leads to a downstream shift of the chemiluminescence intensities compared to the heat release distribution. Lauer and Sattelmayer [16] concluded that these effects are not limited to the flames under investigation in their study. Similar effects have to be expected in general in turbulent flames.

Purpose of the study

The non-linear influence of turbulence on chemiluminescence intensities has to be considered to obtain reliable turbulent flame heat release information from chemiluminescence. The flames under investigation in this study can be described with the flamelet concept, which assumes a local one-dimensional flame structure. Turbulence increases the flame surface and affects the local flame structure through straining of the flamelets [17].

In this study a model based method to obtain the heat release rate distribution of a lean turbulent flame from its chemiluminescent emissions is presented. Time resolved PIV measurements are used to obtain the input parameters for a strain rate model proposed by Yeung et al. in 1990 [18]. Additionally, the influence of strain on chemiluminescence intensity and heat release rate is investigated with one-dimensional counterflow flame simulations. The used reaction mechanism includes all relevant chemiluminescence reactions and deactivation processes [19]. The results of the counterflow simulations are linked to the strain rate model from Yeung et al. to characterize the non-linear reduction of the chemiluminescence intensity due to straining of the flamelets. Measured OH* intensities of the flame are then adjusted with the relationship obtained before to deliver heat release rate proportional intensities. The results are compared with heat release rate distributions obtained with the energy balance method developed earlier [16].

The presented model based method allows for a reliable determination of the heat release rate distribution in lean turbulent flames via OH* chemiluminescence. The required experimental effort is limited to PIV and chemiluminescence measurements. Thus, the presented method can be easily applied to research fields like thermoacoustics or complex test rigs close to technical application, in which expensive LIF-based measurement techniques, like heat release imaging or the method presented by Lauer and Sattelmayer earlier [16], cannot be applied.

The study presented below is focused on premixed and partially premixed flames.

Outline of the study

In the next sections the experimental setup and diagnostics of this study are presented. Then, the strain rate model is described and its applicability in the present study is discussed. Thereafter, the counterflow flame simulations are presented, followed by the chemiluminescence intensity correction procedure and the results. The study is concluded with a summary.

Test rig

The investigated flame is a turbulent, atmospheric swirl flame. The modular burner consists of a tangential swirler, a conical nozzle, and a cylindric center body. The inner diameter of the nozzle is $D = 40\,\text{mm}$, the diameter of the center body is $d = 16\,\text{mm}$. The swirl number can be adjusted by partially blocking the tangential slits of the swirler, but was held constant at 0.55 in this study. Fuel is natural gas with a methane content of 98%. The thermal power can be adjusted between 10 kW and 120 kW, the equivalence ratio ϕ between 0.5 and 1.25.

In the present study the fuel mass flow is equivalent to 60kW thermal power, and the equivalence ratio is varied in six steps from $\phi = 0.63$ to $\phi = 0.91$. The Reynolds number in the burner nozzle ranges from 30,100 ($\phi = 0.91$) to 43,600 ($\phi = 0.63$). Fuel and air are externally premixed to avoid any mixture fluctuations in the burner. A sketch of the test rig is shown in Fig. 1, left hand side. The test rig is operated with non-preheated air-fuel mixture in the present study.

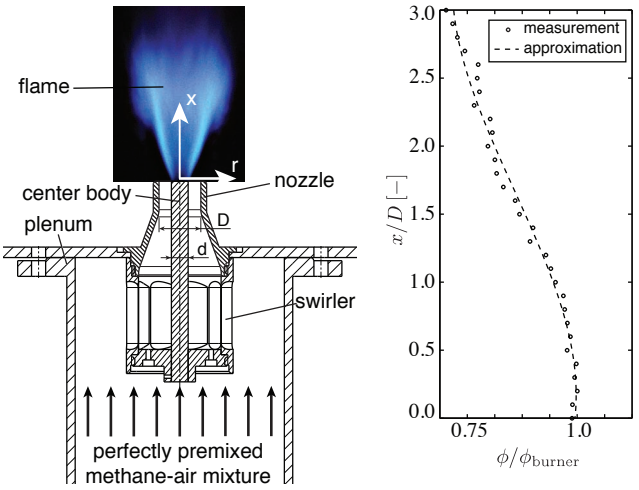

FIGURE 1. LEFT HAND SIDE: SKETCH OF THE TEST RIG. RIGHT HAND SIDE: TYPICAL AXIAL EQUIVALENCE RATIO PROFILE DUE TO AMBIENT AIR ENTRAINMENT [7].

The flame is burning unconfined without a combustion chamber. This causes a non-constant equivalence ratio in the flame. As Wäsle et al. [20] have shown, a linear increase of the axial mass flow downstream of the burner exit occurs due to turbulent mixing in the shear layer between the swirled flow and the quiescent ambient air. As a consequence the mixture becomes leaner with increasing axial distance from the burner nozzle. This property of the flame is used to study the influence of equivalence ratio gradients in partially premixed flames, or to mimic the admixing of air in confined gas turbine flames leading to mixture gradients. A typical axial equivalence ratio profile is shown on the right hand side of Fig. 1. The equivalence ratios shown are normalized with the equivalence ratio in the burner exit plane ϕ_{burner}.

MEASUREMENT TECHNIQUES

In this section, the measurement techniques and data evaluation procedures are described. The most important quantity in this study is the spatially resolved OH* chemiluminescence. The time resolved velocity of the flow is needed to obtain the required input parameters for the strain rate model, which is described later. Another important input parameter for the strain rate model is the local equivalence ratio of the flame, which is measured via the OH*/CH* chemiluminescence ratio. All data are acquired in a flame center-plane.

Chemiluminescence

Image intensified cameras and bandpass filters are used to measure the two-dimensional, spatially resolved chemiluminescence of the flame. However, in hydrocarbon flames bandpass filtered measurements are always a superposition of the desired chemiluminescence signal from OH* or CH* and the broadband emissions from CO_2*. This can be seen in Fig. 2: The figure shows a typical chemiluminescence spectrum of an atmospheric, turbulent methane-air flame. The narrowband emissions from the radicals (OH* around 285 nm and 310 nm, CH* around 390 nm and 430 nm and C_2* around 470 nm) are superimposed by the broadband emissions from CO_2* (dashed line).

The dotted line is the transmission curve of a typical narrowband interference filter for OH* measurements. The gray area is the integral chemiluminescence from the $X^2\Pi_i \leftarrow A^2\Sigma^+(\Delta v = 0)$ transition of OH* to be recovered from the measurements.

It can be seen in Fig. 2 that a significant portion of the light transmitted by the filter is CO_2* chemiluminescence. In turbulent flames, the CO_2* contribution in the measurement signal can be of the same order, or even exceed the contribution from radical species. A measurement and data evaluation procedure developed by Lauer and Sattelmayer in an earlier study is used to separate the emissions of the radicals and CO_2* in bandpass filtered measurements. All details of this procedure are presented in [16].

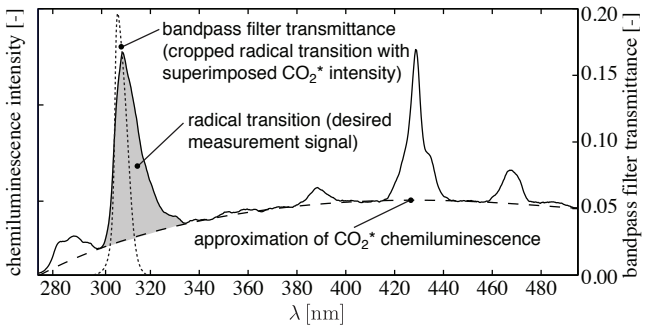

FIGURE 2. TYPICAL CHEMILUMINESCENCE SPECTRUM OF AN ATMOSPHERIC, TURBULENT METHANE-AIR FLAME. THE DASHED LINE IS AN APPROXIAMTION FOR THE BROADBAND EMISSION FROM CO_2*. THE DOTTED LINE IS THE TRANSMISSION CURVE OF A TYPICAL OH* FILTER. THE GRAY AREA REPRESENTS THE DESIRED MEASUREMENT SIGNAL.

All chemiluminescence measurements are line-of-sight integrated. Thus, in order to obtain spatially resolved intensities the measurement signals must be deconvoluted [21]. Due to the turbulent character of the flames under investigation this can be only done with the (rotational symmetric) time-averaged chemiluminescence signals. Since we present a statistical correction method in this paper, the time-averaged chemiluminescence signals in the flame mid-plane are sufficient for the application of the method.

Time resolved velocities

The velocity of the reacting flow in the flame mid-plane is measured with particle image velocimetry, using a high speed double cavity Nd:YLF laser (527 nm, 10 mJ/pulse). The light sheet width is approximately 2 mm. The laser pulses are separated by 20 μs, and the system is operated with a repetition rate of 1 kHz. A high speed camera with a 1024x1024 pixel CMOS sensor is used, together with an 85 mm focal length camera lens with a maximum aperture of 1:1.4. However, the aperture is closed to 5.6 to increase the depth of focus. Additionally, a 532 nm bandpass filter with 10 nm half-transmission bandwidth is used to suppress disturbing chemiluminescence from the flame. TiO_2 particles are chosen as tracers, due to their high temperature resistance.

The double frames are analyzed with a commercial software. A four-step adaptive cross-correlation with 8x8 pixel interrogation area size and 4 pixel separation is used. This results in 255x255 instantaneous velocity vectors with approximately 1 mm spatial resolution. For each operation point, 1024 image pairs are analyzed. From these data, the macroscopic turbulence properties of the reacting flow can be calculated: The spatially resolved rms (root mean square) value of the turbulent velocity fluctuation $u'_{i,\mathrm{rms}}$, and the integral length scale of turbulence l_t.

Turbulent velocity fluctuation The rms value of the turbulent velocity fluctuation $u'_{i,\mathrm{rms}}$ is calculated from the N instantaneous velocity vectors [22]:

$$u'_{i,\mathrm{rms}}(\vec{x}) = \langle u_i'^2(\vec{x})\rangle_t^{0.5} = \left(\frac{\sum_{n=1}^{N} \left(u_{i,n}(\vec{x}) - \langle u_i(\vec{x})\rangle_t \right)^2}{N-1} \right)^{0.5} \quad (1)$$

Integral length scale The integral length scale l_t is defined as the integral of the two-point correlation function $R_{u_i u_i}(r_i)$, normalized with $u'^2_{i,\mathrm{rms}}$ [23]:

$$l_t(\vec{x}) = \int_{r_i=0}^{\infty} \frac{R_{u_i u_i}(\vec{x}, r_i)}{u'^2_{i,\mathrm{rms}}(\vec{x})} dr_i = \int_{r_i=0}^{\infty} \frac{\langle u_i(\vec{x})\, u_i(\vec{x}+\vec{e}_i r_i)\rangle_t}{u'^2_{i,\mathrm{rms}}(\vec{x})} dr_i \quad (2)$$

$\vec{e}_i$ is the unit vector. The direct evaluation of Eq. (2) is problematic, because the spatial resolution of the velocity measurement is of the same order of magnitude as the integral length scales. Thus, the integration of Eq. (2) based on experimental data would result in great uncertainties. This problem is solved by describing the normalized two-point correlation analytically with an exponential function [24]:

$$\frac{R_{u_i u_i}(\vec{x}, r_i)}{u'^2_{i,\mathrm{rms}}(\vec{x})} = \exp\left(-\frac{\pi}{4} \left(\frac{r_i}{l_t(\vec{x})} \right)^2 \right) \quad (3)$$

The integral length scale can be determined reliably by fitting the experimental data with the exponential function defined in Eq. (3) with $l_t(\vec{x})$ as the only free parameter. Figure 3 shows a measured two-point correlation with the corresponding fit and the determined integral length scale of turbulence.

Local equivalence ratio

The local equivalence ratio is measured via the OH*/CH* chemiluminescence ratio. A number of studies have shown the applicability of this technique for laminar and turbulent flames [15, 25–29]. OH* and CH* chemiluminescence is measured sequentially as described in [16]. The local equivalence ratio is calculated from the chemiluminescence ratio with an empirically determined calibration curve, which was determined from confined flames without equivalence ratio gradients.

Although the local equivalence ratio is fluctuating due to the turbulent character of the mixing processes in the shear layer between the swirling flow and the quiescent ambient air, it is approximated with the time-averaged value. This approximation is tenable, because the fluctuations can be expected to be small.

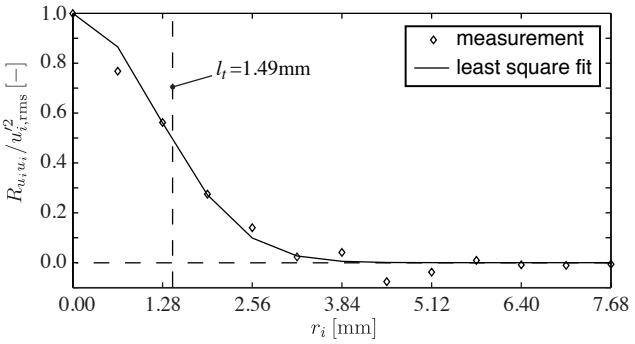

FIGURE 3. MEASURED TWO-POINT CORRELATION, FITTED WITH THE EXPONENTIAL FUNCTION DEFINED IN EQ. (3) AND THE DETERMINED INTEGRAL LENGTH SCALE.

However, if the statistics of the equivalence ratio fluctuations are known, they can be easily taken into account in the presented correction method.

Spatially resolved heat release rate

For the validation of the chemiluminescence correction method, the time-averaged, spatially resolved heat release rate has to be measured by a precise reference method. A measurement technique developed in an earlier study is used for this purpose [26]: The local net heat release rate of the flame is balanced with the increase of the fluid's sensible enthalpy based on the first law of thermodynamics (Fig. 4).

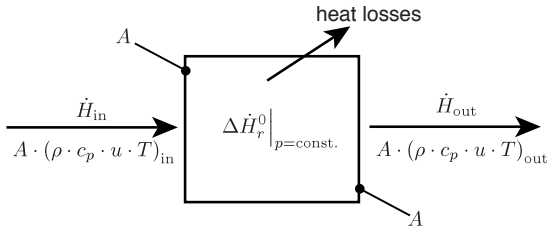

FIGURE 4. ENERGETIC SKETCH OF A FINITE FLAME VOLUME. THE HEAT LOSSES ARE NEGLIGIBLE IN THIS STUDY [26].

For the flames under investigation in this study the following equation can be derived [26]:

$$\dot{q}_{net} = \rho(\phi,c) \cdot c_{\mathrm{p}}(\phi,c) \cdot (\vec{u} \circ \nabla T(\phi,c)) \tag{4}$$

The volumetric net heat release rate of the flame $\dot{q}_{net}$ is a function of the density ρ of the fluid, the isobaric heat capacity c_{p}, the fluid velocity $\vec{u}$, and the temperature gradient ∇T. Density, heat capacity, and temperature are functions of the fluid composition, which can be described by the local equivalence ratio ϕ of the mixture and progress variable of combustion c. ϕ and c can be measured via the OH*/CH* ratio and OH-PLIF.

All details about this measurement method and a detailed plausibility discussion of the results are presented by Lauer and Sattelmayer [16, 26].

STRAIN RATE MODEL

In this section the statistical model for the tangential strain rate, which is used in the present study, is described. In the first part the basic model is introduced. In the second part the applicability of the model to the flames under investigation in the present study is discussed.

Statistical description of the strain rate

The tangential strain rate model used in this study was developed by Yeung et al. in 1990 [18]. The model is based on the direct numerical simulation (DNS) of constant-property, homogeneous, isotropic turbulence. From these simulations the statistics of strain rate in the tangential plane of predefined surfaces in the fluid were extracted. The details of the simulation are given by Yeung and Pope in [30]. The Taylor scale Reynolds-number Re_λ of the simulations ranged from 38 to 93.

It was shown that the tangential strain rate statistics are a function of the propagation speed of the investigated surfaces. In summary it was demonstrated that the strain rates of a slowly propagating surface are well represented by the strain rate distribution of a material surface, and that the strain rates of a rapidly propagating surface are well represented by the strain rate distribution of a randomly oriented surface. Furthermore, it was shown by Yeung et al. that the probability density function $p(a)$ of the strain rate shows no significant Reynolds-number dependance when the Kolmogorov time scale τ_η is used for normalization, and that the strain rate distributions can be approximated very accurately with gaussian functions.

The mean strain rate of a randomly oriented surface $\langle \alpha \rangle$ is zero, whereas a material surface has a positive mean strain rate $\langle a \rangle = 0.280/\tau_\eta$. The standard deviations of the strain rate distributions for randomly oriented and material surfaces are $\sigma_\alpha = 0.257/\tau_\eta$ and $\sigma_a = 0.342/\tau_\eta$. The parameters of the gaussian approximations are summarized in Tab. 1.

Applicability to turbulent flames

A simulation of constant property, homogeneous, isotropic turbulence is a very limiting approximation for a turbulent flame. Thus, it has to be discussed, whether the statistical strain rate distributions reported by Yeung et al. can be used to describe the straining of (partially) premixed flames. Further, it must be investigated, whether flamelets can be described as material or randomly oriented surfaces.

Re_λ	$\langle a \rangle \cdot \tau_\eta$	$\sigma_a \cdot \tau_\eta$	$\langle \alpha \rangle \cdot \tau_\eta$	$\sigma_\alpha \cdot \tau_\eta$
38	0.287	0.344	0	0.257
63	0.275	0.345	0	0.255
90	0.273	0.339	0	0.257
93	0.283	0.341	0	0.257
average	0.280	0.342	0	0.257

TABLE 1. PARAMETERS OF THE GAUSSIAN DESCRIPTIONS OF THE TANGENTIAL STRAIN RATE PDFS OBTAINED BY YEUNG ET AL. [18]. $\langle a \rangle$ AND σ_a REFER TO A MATERIAL SURFACE, $\langle \alpha \rangle$ AND σ_α TO A RANDOMLY ORIENTED SURFACE.

Constant property, homogeneous flow In accordance with Pope [31] and Bradley et al. [32], the turbulence ahead of a premixed flame causes the main contribution to flame straining. Thus, the statistical strain rate distributions can be calculated from the turbulent properties of the unburnt mixture, in which the flame propagates. The unburnt mixture can be approximated as a constant property, homogeneous flow. Furthermore, Bradley et al. [32] used the statistical strain rate distributions from Yeung et al. [18] to predict turbulent burning velocities in fan stirred bombs, and compared these with experimental data. The very good agreement between prediction and experimental data indicates the validity of the strain rate model for premixed combustion processes.

In 1998 Chen and Im [33] obtained statistical strain rate distributions from 2-dimensional DNS of premixed, unsteady methane-air flames with a detailed C_1 mechanism for the methane oxidation. Stoichiometric and lean mixtures were investigated. The results are in good agreement with those from Yeung et al., which also confirms the validity of the model for premixed, isotropic turbulent flames.

It can be concluded that although the strain rate distributions presented by Yeung et al. [18] were obtained from simulations of a non-reacting flow, the distributions reliably describe the straining of isotropic turbulent flames.

Isotropic turbulence Further, it must be investigated, whether the flames under investigation in the present study satisfy the assumption of isotropic turbulence. In isotropic turbulence the time-averaged product of orthogonal components of the velocity fluctuation equals zero [34]:

$$\langle u_i' u_j' \rangle_t = 0,\ i \neq j \tag{5}$$

The right hand side of Fig. 5 shows the time-averaged product of the radial and axial components of the velocity fluctuation $\langle u_x' u_r' \rangle_t$. For comparison $\langle u_x' u_x' \rangle_t$ is shown on the left hand side.

It can be seen that Eq. (5) is not exactly satisfied, thus the macroscopic turbulence is not exactly isotropic. This has to be expected for any flame in a flow field with a significant mean

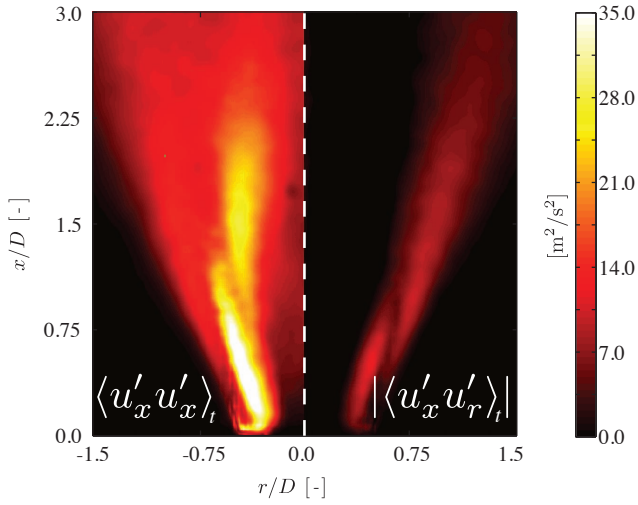

FIGURE 5. COMPARISON OF THE TIME-AVERAGED PRODUCT OF THE RADIAL AND AXIAL COMPONENTS OF THE VELOCITY FLUCTUATION (RIGHT HAND SIDE) WITH $\langle u_x'^2 \rangle_t$ (LEFT HAND SIDE).

velocity. However, since the absolute value of $\langle u_x' u_r' \rangle_t$ is significantly lower than $\langle u_x' u_x' \rangle_t$, it is tenable to approximate the macroscopic turbulence in the flame as isotropic[1]. Moreover, the straining of the flamelets is not caused by the macroscopic turbulence of the flow field, but by the small scale turbulence. Based on Kolmogorov's hypothesis of local isotropy, the small scale turbulence can be considered to be isotropic in any case [35][2].

Material and randomly oriented surface The turbulent flamelet must be characterized as material or randomly oriented surface in order to choose the appropriate strain rate distribution from the model of Yeung et al.

Per definition a material surface does not propagate by itself, it is only passively convected by turbulence, whereas a randomly oriented surface is propagating independently from turbulence [18]. As a first approximation, a flamelet is propagating with the laminar flame speed in the turbulent flow. On the one hand, the propagation with the laminar flame speed is an indicator for a randomly oriented surface. On the other hand, the flamelet is convected and reorientated by the turbulence, which is an indicator for a material surface. Yeung et al. discuss this question in great detail [18]. They come to the conclusion that a flamelet can be assumed to be a material surface, if its propagation velocity is small compared to the time scale by which it

[1]Also other criteria for the macroscopic isotropy of the turbulence, like $\langle u_i u_i \rangle_t = \langle u_j u_j \rangle_t, i \neq j$ and the independence of the integral length scale on direction, have been checked with comparable results and conclusions.

[2]First published in Russian in *Dokl. Akad. Nauk SSSR* (1941) **30**(4). Paper received December 28th 1940.

is reoriented by turbulence. Finally, Yeung et al. conclude that a flamelet can be considered as a material surface, if the laminar flame speed u_l is smaller than the Kolmogorov velocity v_η. The Kolmogorov velocity is defined as [35]:

$$v_\eta = (\varepsilon\,\nu)^{1/4}, \text{ with } \varepsilon = 15\,\nu\,\frac{u'^2_{x,\mathrm{rms}}}{l_\lambda^2} \tag{6}$$

ν denotes the kinematic viscosity of the unburnt mixture and l_λ the Taylor length scale. The Taylor length scale can be obtained geometrically by constructing a parabola which osculates the normalized two-point correlation function at $r_i = 0$. The intersection of this parabola with the r_i-axis is the Taylor length scale l_λ [23]. Figure 6 shows a sketch of the geometrical determination of l_λ.

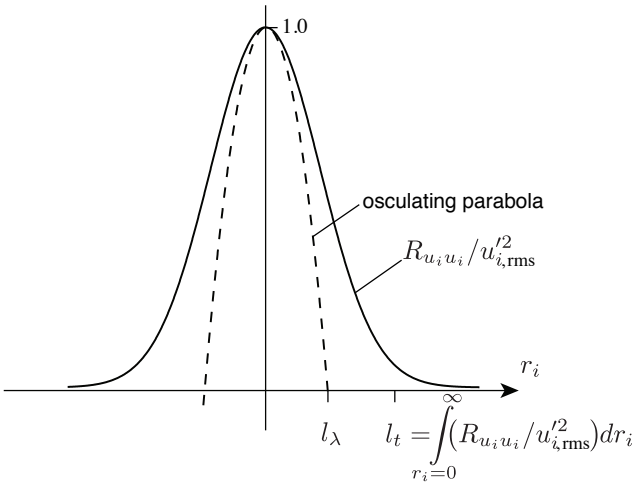

FIGURE 6. SKETCH OF THE TWO-POINT CORRELATION FUNCTION AND THE PARABOLA DEFINING THE TAYLOR LENGTH SCALE.

However, the spatial resolution of the PIV measurement is too low to determine the slope and curvature of the two-point correlation function reliably. Because of this, the Taylor length scale is estimated from the integral length scale based on former studies found in literature:

In 1935 Taylor [36] investigated grid generated turbulence. With Constant Temperature Anemometer measurements he obtained the relation $l_\lambda \approx 0.5\,l_t$. Girimaji and Pope [37] obtained the integral length scale and the Taylor length scale from their DNS. They determined a range of $l_\lambda = 0.33\,l_t$ to $l_\lambda = 0.5\,l_t$, depending on the turbulent Reynolds-number of the flow. Steinberg and Driscoll [38] characterized the Taylor length scale with Laser Doppler Velocimetry in 2009 and obtaind $l_\lambda \approx 0.63\,l_t$. Based on these results the Taylor length scale is approximated with $l_\lambda = 0.5\,l_t$ in the present study.

With this approximation for the Taylor length scale, the Kolmogorov velocity can be calculated and compared to the laminar burning velocity to determine, whether the flames under investigation in the present study can be considered as material or randomly oriented surfaces. Figure 7 shows the Kolmogorov velocity (left hand side) for a 60 kW, stoichiometric flame in comparison with the local laminar flame speed (right hand side). The laminar flame speed is calculated from the measured local equivalence ratio [39]. The comparison reveals that the Kolmogorov velocity is always higher than the local laminar flame speed for this case.

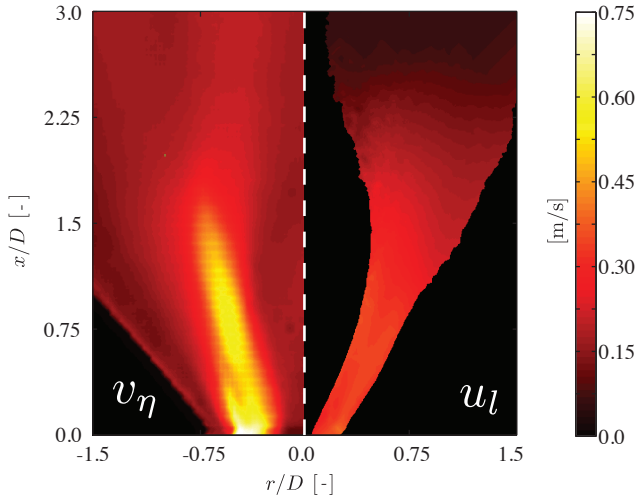

FIGURE 7. COMPARISON OF THE KOLMOGOROV VELOCITY v_η (LEFT HAND SIDE) AND THE LAMINAR FLAME SPEED u_l (RIGHT HAND SIDE). SINCE THE LAMINAR FLAME SPEED IS OBTAINED FROM CHEMILUMINESCENCE MEASUREMENTS, IT CAN BE DETERMINED ONLY INREGIONS WHERE CHEMILUMINESCENCE IS EMITTED, WHEREAS THE KOLMOGOROV VELOCITY, DETERMINED FROM PIV MEASUREMENTS, CAN BE CALCULATED IN THE COMPLETE FLAME MID-PLANE.

As the thermal power of the flame is kept constant in this study, the lean flames correspond to larger air mass flows and thus higher flow velocities. This results in increasing turbulent velocity fluctuations with decreasing equivalence ratio, whereas the Taylor length scale shows no significant equivalence dependency, resulting in increasing Kolmogorov velocities with decreasing equivalence ratio. On the other hand, the laminar flame speed is decreasing with decreasing equivalence ratio. Since the condition $v_\eta > u_l$ for material surfaces is already satisfied for the stoichiometric flame, all lean flames under investigation in this study can be considered as material surfaces[3].

[3] In a detailed study Bradley et al. found that the strain rate distributions show a continuous transition between the distributions of randomly oriented and mate-

Summary of strain rate model

It was shown that for the flames under investigation in this study the strain rate model proposed by Yeung et al. [18] can be applied. Further, it was shown that the flames can be considered as material surfaces. As the consequence, the statistical distribution $p(\vec{x},a)$ of the strain rate a of the flames can be approximated as

$$p(\vec{x},a) = \frac{\tau_\eta(\vec{x})}{\sqrt{2\pi}\,0.342} \exp\left(-\frac{1}{2}\left(\frac{a\,\tau_\eta(\vec{x}) - 0.280}{0.342}\right)^2\right) \qquad (7)$$

with [35]

$$\tau_\eta(\vec{x}) = \left(15\,\frac{u'^2_{x,\mathrm{rms}}(\vec{x})}{l^2_\lambda(\vec{x})}\right)^{-0.5} \qquad (8)$$

COUNTERFLOW FLAME CALCULATIONS

The non-linear effect of strain on chemiluminescence intensities has to be taken into account in order to obtain reliable heat release rate information from OH* measurements. However, this effect is hardly accessible by experiments. Thus, numerical simulations of one-dimensional counterflow flames with detailed chemistry are done to obtain the desired relationship between strain rate, OH* intensities, and volumetric heat release rate. In the next section this relationship is linked with the strain rate model presented before.

Numerical setup

The counterflow flame calculations are done with the reaction mechanism from Kathorita et al. [19] that includes all relevant chemiluminescence reactions and deactivation processes. In the simulation, planar jets of fresh gas and burnt gases are opposed. The flames stabilize near the stagnation point between the two jets. This so-called fresh-to-burnt setup is chosen, because it is, compared the the fresh-to-fresh setup (two opposed jets of fresh gas with a twin flame in between), the more realistic description for premixed and partially premixed flamelets [32].

The simulation is done in a fully infinite domain with strain rate as parameter. Nine equivalence ratios from $\phi = 0.56$ to $\phi = 1.0$ and 18 strain rates from $a = 500$ to $a = 20,000$ are calculated. Boundary condition on the fresh gas side are the volume fractions of O_2, N_2 and CH_4, corresponding to the equivalence ratio of the flame, and the unburnt temperature of the mixture. On the burnt side the boundary conditions are zero gradients for the volume fractions of all species and the temperature.

For each case an initial solution is calculated with a C_1-mechanism with 16 species and 46 reactions. Then, the more detailed mechanism of Kathrotia et al. with 69 species and 496 reactions [19] is used. The simulations are started in unsteady mode with an initial time step of 10^{-8} s. The time step size is gradually increased to a maximum of 10^3 s. After 10^4 s the simulations are stopped and are used as initial solutions for the final, stationary calculations.

Data processing

From the results of the simulations the profiles of the volumetric heat release rate $\dot{q}_x$ and the mole fraction of OH* $X_{\mathrm{OH}^*,x}$ were extracted. $X_{\mathrm{OH}^*,x}$ is directly proportional to the volumetric OH*-intensity $i_{\mathrm{OH}^*,x}$, with the Einstein coefficient of spontaneous emission as proportionality factor. From these quantities the strain rate and equivalence ratio dependent proportionality factor $C(a,\phi)$ between heat release rate and OH*-intensity is defined:

$$C(a,\phi) = \frac{\dot{q}(a,\phi)}{i_{\mathrm{OH}^*}(a,\phi)} = \frac{\int_{-\infty}^{\infty} \dot{q}_x(a,\phi,x)dx}{\int_{-\infty}^{\infty} i_{OH^*,x}(a,\phi,x)dx} \qquad (9)$$

A flamelet cannot experience arbitrary strain rates. Above a certain, equivalence ratio dependent value $a_q(\phi)$, combustion will be quenched. For symmetric (fresh-to-fresh configuration) counterflow flames it was shown in several studies that the heat release profile of the flame hardly changes with strain rate, until the quenching strain rate is reached. Above the quenching strain rate there is no heat release. For fresh-to-burnt counterflow flames the heat release rate profiles change in a more gradual way with increasing strain rate. Therefore, the quenching strain rate is more difficult to define [32]. A suitable quenching criterion in the present study is the strain rate, for which the integral heat release rate of the flame drops below two percent of the unstrained value.

The result of the counterflow flame calculations is a lookup table for the proportionality factor between heat release rate and OH*-intensity with strain rate and equivalence ratio as parameters. Values between the calculated data points are interpolated bicubically, values above the quenching strain rate are not defined and thus not taken into account.

It is important to note that the calculated lookup table for $C(a,\phi)$ is specific for fuel, pressure, and preheating of the flame under investigation in this study. A change of one of these properties requires a new set of counterflow simulations with matching boundary conditions.

---

rial surfaces, depending on the ratio of Kolmogorov velocity and laminar flame speed. They defined empirical exponential forms for $\langle a \rangle$ and σ_a to take this transition into account [32]. Since in the present study the condition $v_\eta > u_l$ is clearly satisfied, the simpler relationship defined by Yeung et al. [18] is used.

OH* CORRECTION METHOD AND RESULTS

In this section the statistical strain rate distributions obtained from the model of Yeung et al. and the PIV measurements are linked to the lookup table from the one-dimensional counterflow simulations. The purpose is to obtain a correction factor which accounts for the non-linear relationships between OH*-intensity, heat release rate, and strain rate. Such a factor can be interpreted as a representative, strain rate distribution averaged proportionality factor between OH*-intensity and heat release rate for a specific equivalence ratio.

In the first subsection the linking of the strain rate distributions and the lookup table is described. In the second subsection the results of the correction method are presented.

Evaluation of strain rate pdfs

The strain rate distribution (Eq. (7)) is evaluated in each point of the flame mid-plane. The Kolmogorov time scale is calculated from the PIV measurements. It can be seen easily that approximately 20.6 percent of the obtained strain rates are negative. Negative strain rates are very difficult to access by both, experiment and simulation. Thus, for negative strain rates the approximation proposed by Bradley et al. with the unstrained value is used [32].

The representative, strain rate averaged proportionality factor $\langle C(\phi)\rangle_a$ between the time averaged heat release rate and chemiluminescence intensity is calculated as:

$$\langle C(\phi)\rangle_a = \frac{\int_{-\infty}^{a_q(\phi)} C(a,\phi)p(a)da}{\int_{-\infty}^{a_q(\phi)} p(a)da} \tag{10}$$

The numerator of the right hand side of Eq. (10) is the strain rate distribution weighted average of the proportionality factor. Since $C(a,\phi)$ is only defined for strain rates smaller than the quenching criterion $a_q(\phi)$, the integral is evaluated in the limits $-\infty$ and $a_q(\phi)$. The denominator accounts for this clipping of the gaussian distribution by re-normalizing the numerator with the integral of all probabilities between $-\infty$ and $a_q(\phi)$. $\langle C(\phi)\rangle_a$ represents the strain rate distribution averaged proportionality factor between measured OH*-chemiluminescence intensity and heat release rate for all unquenched states of the flame. Quenched states are not taken into account in the proportionality factor, because their contribution is captured in the measured OH*-intensities. If the proportionality factor would not be re-normalized, the effect of quenching would be considered twice.

Since the turbulent properties and the equivalence ratio of the flame are not constant, the proportionality factor $\langle C(\phi)\rangle_a$ has to be calculated in each point of the flame mid-plane and for each operation point using Eq. (10).

Results

The calculated proportionality factor correlates the measured, time-averaged OH*-intensity with the desired time averaged heat release rate of the flame:

$$\langle C\rangle_a \langle i_{OH^*}\rangle_t \sim \langle \dot{q}\rangle_t \tag{11}$$

The measured OH*-intensities are no quantitative photon count of the light emission of the flame, but rather a relative measurement signal. Because of this the corrected OH*-intensities are only proportional to the heat release rate. However, if the integral heat release rate of the flame is known, for example from the burnt fuel mass flow, the corrected chemiluminescence intensities can be scaled to match this value.

Figure 8 shows the result of the correction procedure for the $\phi = 0.67$ operation point. In the upper part of the figure the heat release rate, measured with the energy balance method described in [16], is shown on the left hand side. In the middle the measured OH* chemiluminescence intensities, and on the right hand side the strain rate corrected OH*-intensities are shown.

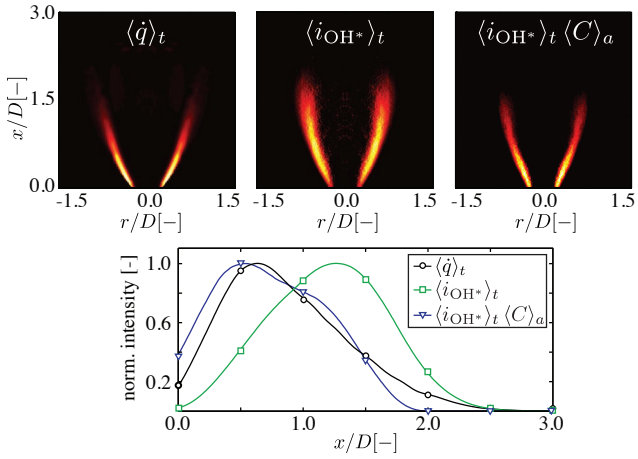

FIGURE 8. RESULT OF THE INTENSITY CORRECTION PROCEDURE FOR THE $\phi = 0.67$ OPERATION POINT. IN THE UPPER PART THE LOCAL HEAT RELEASE RATE, THE MEASURED OH* INTENSITIES, AND THE CORRECTED OH* INTENSITIES ARE SHOWN. THE LOWER PART SHOWS THE CORRESPONDING AXIAL PROFILES.

It can be clearly seen that the correction method shifts the intensities closer to the burner exit, which results in a more compact flame with high heat release rate at the burner exit. The corrected intensities are a good approximation for the heat release distribution of the flame, the effect of turbulence reported by Lauer and Sattelmayer [16] is captured.

This becomes even more obvious, when the intensities are integrated in radial direction to obtain the one-dimensional axial profiles (Fig. 8, lower part). It can be seen that the axial

profile of the corrected OH*-intensities is in very good agreement with the real heat release profile. It can be concluded that the corrected OH*-intensities allow a much better assessment of the heat release rate distribution of the flame than the commonly used uncorrected OH*-intensities.

The $\phi = 0.67$ operation point is representative for all six investigated lean operation points ($\phi = 0.63$ - $\phi = 0.91$). For all lean operation points the correction procedure results in compacter flames and a very good agreement of the one-dimensional profiles.

CONCLUSION

A new, model based method has been presented that delivers spatially resolved, heat release rate proportional OH*-chemiluminescence intensities of lean turbulent flames. With a strain rate model proposed by Pope and co-workers in 1990 and appropriate one-dimensional counterflow flame calculations, measured OH* intensity distributions were corrected to exhibit heat release rate proportional intensities. The results of this correction method were compared with measured heat release rate distributions.

The corrected chemiluminescence intensities of all investigated lean flames were in very good agreement with the real heat release rate distributions. In comparison with the commonly used approximation of the heat release rate with uncorrected OH*-intensities, the presented method represents a significant improvement in the lean regime, which is of outstanding technical relevance for low emission combustion techniques.

The proposed method is based on a statistical strain rate model, evaluated with time resolved PIV measurements, and one-dimensional counterflow flame simulations, which are used to obtain the basic relationship between heat release rate, strain rate and OH* chemiluminescence intensity. Thus, the presented method is universal and can be applied to a wide range of flame studies with moderate effort to provide accurate heat release rate distributions for lean premixed and partially premixed flames. The method can be enhanced easily to capture the influence of fuel variations (for example H_2 enriched fuels), preheating temperature, or pressure by appropriate counterflow flame simulations. Also equivalence ratio fluctuations can easily be taken into account.

ACKNOWLEDGMENT

The authors wish to thank Ms. Trupti Kathrotia and Dr. Uwe Riedel from the DLR and University of Stuttgart for providing the used reaction mechanism.

The authors also gratefully acknowledge the financial support provided by the DFG through the research unit "Chemilumineszenz und Wärmefreisetzung" and the National Science Foundation grant number CBET-0832561.

REFERENCES

[1] Auer, M., Gebauer, C., Mösl, K., Hirsch, C., and Sattelmayer, T., 2005. "Feedback of combustion instabilities on the injection of gaseous fuel". *J. Eng. Gas Turbines Power,* ***127***, pp. 748–754.

[2] Auer, M., Hirsch, C., and Sattelmayer, T., 2005. "Influence of the interaction of equivalence ratio and mass flow fluctuation on flame dynamics". In Proceedings of the ASME Turbo Expo 2005.

[3] Freitag, E., Konle, H., Lauer, M., Hirsch, C., and Sattelmayer, T., 2006. "Pressure influence on the flame transfer function of a premixed swirling flame". In Proceedings of the ASME Turbo Expo 2006.

[4] Konle, M., Kiesewetter, F., and Sattelmayer, T., 2008. "Simultaneous high repetition rate PIV-LIF measurements of CIVB driven flashback". *Exp. Fluids,* ***44***, pp. 529–538.

[5] Konle, M., and Sattelmayer, T., 2010. "Time scale model for the prediction of the onset of flame flashback driven by combustion induced vortex breakdown". *J. Eng. Gas Turbines Power,* ***132/4***, pp. 041503/1–6.

[6] Wäsle, J., Winkler, A., and Sattelmayer, T., 2005. "Spatial coherence of the heat release fluctuations in turbulent jet and swirl flames". *Flow Turbul. Combust.,* ***75***, pp. 29–50.

[7] Wäsle, J., Winkler, A., Lauer, M., and Sattelmayer, T., 2007. "Combustion noise modeling using chemiluminescence data as indicator for the heat release distribution". In Proceedings of European Combustion Meeting, 2007.

[8] Ayoola, B., Balachandran, R., Frank, J., Mastorakos, E., and Kaminski, C., 2006. "Spatially resolved heat release rate measurements in turbulent premixed flames". *Combust. Flame,* ***144***, pp. 1–16.

[9] Balachandran, R., Ayoola, B., Kaminski, C., Dowling, A., and Mastorakos, E., 2005. "Experimental investigation of the nonlinear response of turbulent premixed flames to imposed inlet velocity oscillations". *Combust. Flame,* ***143***, pp. 37–55.

[10] Clark, T., and Bittker, D., 1954. A study of the radiation from laminar and turbulent open propane-air flames as a function of flame area, equivalence ratio, and fuel flow rate. Tech. Rep. NACA RM E54F29, National Advisory Commettee for Aeronautics, Lewis Flight Propulsion Laboratory Cleveland, Ohio.

[11] John, R., and Summerfield, M., 1957. "Effect of turbulence on radiation intensity from propane-air flames". *Jet Propul.,* ***27***, pp. 169–179.

[12] Hurle, I., Price, R., Sugden, T., and Thomas, A., 1968. "Sound emission from open turbulent premixed flames". *Proc. R. Soc. London, Ser. A,* ***303***, pp. 409–427.

[13] Samaniego, J.-M., Egolfopoulos, F., and Bowman, C., 1995. "CO_2* chemiluminescence in premixed flames". *Combust. Sci. Technol.,* ***109***, pp. 183–203.

[14] Haber, L., Vandsburger, U., Saunders, W., and Khanna,

V., 2000. "An examination of the relationship between chemiluminescent light emissions and heat release rate under non-adiabatic conditions". In Proceedings of International Gas Turbine Institute 2000.

[15] Hardalupas, Y., and Orain, M., 2004. "Local measurements of the time-dependent heat release rate and equivalence ratio using chemiluminescent emission from a flame". *Combust. Flame,* ***139***, pp. 188–207.

[16] Lauer, M., and Sattelmayer, T., 2010. "On the adequacy of chemiluminescence as a measure for heat release in turbulent flames with mixture gradients". *J. Eng. Gas Turbines Power,* ***132/6***, pp. 061502/1–8.

[17] Peters, N., 1986. "Laminar flamelet concepts in turbulent combustion". *Proc. Combust. Inst.,* ***21***, pp. 1231–1250.

[18] Yeung, P., Girimaji, S., and Pope, S., 1990. "Straining and scalar dissipation on material surfaces in turbulence: implications for flamelets". *Combust. Flame,* ***79***, pp. 340–365.

[19] Kathrotia, T., Riedel, U., and Warnatz, J., 2009. "A numerical study on the relation of OH*, CH*, and C_2* chemiluminescence and heat release in premixed methane flames". In Proceedings of the European combustion Meeting, 2009.

[20] Wäsle, J., Winkler, A., Rößle, E., and Sattelmayer, T., 2006. "Development of an annular porous burner for the investigation of adiabatic unconfined flames". In Proceedings of 13th Int Symposium on Applications of Laser Techniques to Fluid Mechanics, 2006.

[21] Dribinski, V., Ossadtchi, A., Mandelshtam, V., and Reisler, H., 2002. "Reconstruction of abel-transformable images: The gaussian basis-set expansion abel transform method". *Rev. Sci. Instrum.,* ***73***, pp. 2634–2642.

[22] Mandel, J., 1984. *The statistical analysis of experimental data*. Dover Publications, Inc., N.Y.

[23] Pope, S., 2000. *Turbulent flows*. Cambridge University Press, Cambridge.

[24] Hinze, J., and Clark (Ed.), B., 1975. *Turbulence (2nd edition)*. McGraw-Hill, U.S.

[25] Lauer, M., and Sattelmayer, T., 2007. "Luftzahlmessung in einer turbulenten Drallflamme auf Basis spektral aufgelöster Chemilumineszenz". In VDI-Berichte 1988, 2007, pp. 735–741.

[26] Lauer, M., and Sattelmayer, T., 2008. "Heat release calculation in a turbulent swirl flame from laser and chemiluminescence measurements". In 14th Int Symp on Applications of Laser Techniques to Fluid Mechanics, 2008.

[27] Haber, L., 2000. "An investigation into the origin, measurement and application of chemiluminescent light emissions from premixed flames". Master's thesis, Virginia Polytechnic Institute and State University.

[28] Nori, V., and Seitzman, J., 2007. "Chemiluminescence measurements and modeling in syngas, methane and jet-a fueled combustors". In Proceedings of the 45th AIAA Aerospace Sciences Meeting and Exhibit, 2007.

[29] Guyot, D., Güthe, F., Schuermans, B., Lacarelle, A., and Paschereit, O., 2010. "CH*/OH* chemiluminescence response on an atmospheric premixed flame under varying operation conditions". In Proceedings of ASME Turbo Expo.

[30] Yeung, P., and Pope, S., 1989. "Lagrangian statistics from direct numerical simulations of isotropic turbulence". *J. Fluid Mech.,* ***207***, pp. 531–568.

[31] Pope, S., 1987. "Turbulent premixed flames". *Annu. Rev. Fluid Mech.,* ***19***, pp. 237–270.

[32] Bradley, D., Lau, A., and Lawes, M., 1992. "Flame stretch rate as a determinant of turbulent burning velocity". *Phil. Trans. R. Soc. Lond. A,* ***338***, pp. 359–387.

[33] Chen, J., and Im, H., 1998. "Correlation of flame speed with stretch in turbulent premixed methane/air flames". *Proc. Combust. Inst.,* ***27***, pp. 819–826.

[34] Peters, N., and Batchelor (ed.), G., 2000. *Turbulent combustion*. Cambridge University Press, Cambridge.

[35] Kolmogorov, A., 1991. "The local structure of turbulence in incompressible viscous fluid for very large reynolds numbers". *Proc. R. Soc. London, Ser. A,* ***434***, pp. 9–13.

[36] Taylor, G., 1935. "Statistical theory of turbulence - I". *Proc. R. Soc. London, Ser. A,* ***151***, pp. 421–444.

[37] Girimaji, S., and Pope, S., 1990. "Material-element deformation in isotropic turbulence". *J. Fluid Mech.,* ***220***, pp. 427–458.

[38] Steinberg, A., and Driscoll, J., 2009. "Straining and wrinkling processes during turbulence-premixed flame interaction measured using temporally-resolved diagnostics". *Combust. Flame,* ***156***, pp. 2285–2306.

[39] Turns, S., 2000. *An introduction to combustion (2nd edition)*. McGraw-Hill, U.S.